processes

MDPI

Article

Research on the Mechanism and Prevention Countermeasures of Stuck Coiled Tubing During Coiled Tubing Fracturing in the Junggar Basin

Hongcheng Yin [1], Lan Ren [2], Changyong Guo [1], Xianjiang Chen [1], Qianqiu Ren [2,*], Ran Lin [2] and Qinyue Deng [3]

[1] Development Company, Xinjiang Oilfield Company, PetroChina, Karamay 834000, China
[2] State Key Laboratory of Oil and Gas Reservoir Geology and Exploitation, Southwest Petroleum University, Chengdu 610500, China
[3] Gathering and Transmission Engineering Technology Institute, Southwest Oil & Gas Field Company, PetroChina, Chengdu 610051, China
* Correspondence: renqq_swpu@163.com

Abstract: The coiled tubing (CT) fracturing technology offers advantages such as pressurized dragging operation and maintaining a large borehole diameter after fracturing. However, during fracturing in the conglomerate and volcanic rock reservoirs of the Junggar Basin, CT stuck during retrieval occurs frequently. In this study, a model simulating the variation in the in situ stress field during CT hydraulic fracturing is established based on elastic mechanics and the displacement discontinuity method (DDM). Based on the geological characteristics of conglomerate and volcanic rock reservoirs in the Junggar Basin, and considering engineering parameters such as fracture length and fracture count in CT hydraulic fracturing, this study investigates the variation in the in situ stress during CT hydraulic fracturing and explores the stuck mechanism of CT. An index for fracturing completion is constructed to evaluate the stuck of CT during the fracturing process. With the goal of full stimulation of the horizontal section, a quantitative optimization design is conducted for the fracturing stage spacing and number of stages under different geological conditions, resulting in corresponding charts. The results indicate that the stuck mechanism during CT fracturing is caused by the continuous accumulation of stress induced by hydraulic fractures, leading to stress inversion. The fracturing completion increases with the stage spacing and the original horizontal stress difference. The length of the fractured section first increases and then decreases with the increase in stage spacing, while it increases with the original horizontal stress difference. The research findings can be applied to the optimization design of stage spacing and number of stages for CT hydraulic fracturing in conglomerate and volcanic rock reservoirs of the Junggar Basin, effectively preventing and controlling stuck coiled tubing in CT fracturing.

Keywords: coiled tubing; stuck; induced stress field; fracturing stage spacing; horizontal stress difference

check for updates

Academic Editor: Qingbang Meng

Received: 25 January 2025
Revised: 17 February 2025
Accepted: 26 February 2025
Published: 28 February 2025

Citation: Yin, H.; Ren, L.; Guo, C.; Chen, X.; Ren, Q.; Lin, R.; Deng, Q. Research on the Mechanism and Prevention Countermeasures of Stuck Coiled Tubing During Coiled Tubing Fracturing in the Junggar Basin. *Processes* **2025**, *13*, 701. https://doi.org/10.3390/pr13030701

Copyright: © 2025 by the authors. Licensee MDPI, Basel, Switzerland. This article is an open access article distributed under the terms and conditions of the Creative Commons Attribution (CC BY) license (https://creativecommons.org/licenses/by/4.0/).

1. Introduction

The Junggar Basin covers a total area of 1.3×10^{11} m^2, with proven oil geological reserves of 1.34×10^9 t, and natural gas reserves of 2.554×10^{10} m^3, making it one of the largest oil- and gas-bearing basins in China [1–4]. Currently, the main reservoirs being developed in the Junggar Basin are conglomerate and volcanic rock reservoirs [5,6]. Due to their geological characteristics such as low porosity and low permeability, their natural productivity is generally low, requiring hydraulic fracturing to stimulate the reservoirs and

enhance production capacity [7,8]. The coiled tubing (CT) hydraulic fracturing technology is widely used in the stimulation of conglomerate and volcanic rock reservoirs in the Junggar Basin [9] due to its advantages, such as precise fracture initiation location and controllable single-fracture scale [10,11].

CT can improve construction efficiency in both drilling and fracturing [12]. After the significant success of CT fracturing in Alberta in 1993, scholars have gradually conducted research on CT fracturing [13–15]. Subhash et al. [16] studied the friction characteristics and erosion phenomena of sand-carrying fluids in CT under different parameter conditions, using a combination of experimental testing and computational fluid dynamics simulations. Huang et al. [17] expanded on Subhash's work by conducting flow analysis of the fluid in the CT spiral section and calculating the frictional flow of Newtonian and non-Newtonian fluids. Sun et al. [18] conducted comparative experimental studies on the flow friction characteristics of straight pipes and CT with different sizes and lengths. Xu et al. [19], based on computational fluid dynamics, the discrete phase model, and optimization design theory, performed a numerical simulation of the erosion of a 2.375″ CT wrapped around a drum under the action of fracturing fluid using ANSYS Workbench software. Serguei et al. [20] focused on optimizing the fracturing string design for shallow gas fields in western Canada and altering the equipment geometry of the CT system. Wang et al. [21] developed a new type of pumping CT hydraulic bottom-hole seal trailing section fracturing tool for the efficient development of shale oil in Longdong, China. Liu et al. [22] studied the impact of various factors on the fatigue life of CT. Zhang et al. [23] studied the extension limits of CT based on the buckling model and contact force model. Most research on CT fracturing has focused on the flow friction characteristics of fracturing fluids inside CT, CT structural design, and CT buckling behavior. A few scholars have explored ways to recover stuck CT, but their research primarily focused on proposing solutions for stuck encountered during the post-fracturing wellbore cleaning process [24]. There has been little research on the prediction and prevention of stuck coiled tubing during the fracturing process. In actual field operations, CT can encounter stuck during drilling, which hinders the drilling progress and results in higher drilling costs [25]. Similarly, once CT encounters sticking during retrieval, it can affect the overall fracturing operation efficiency and may even prevent the well from being successfully brought into production.

This study, based on the theory of elasticity, employs the displacement discontinuity method (DDM) to calculate the induced stress generated by hydraulic fractures and establishes a model for the variation in the in situ stress field during CT fracturing. This study investigates the variation in in situ stress field during the CT fracturing, explores the mechanisms of CT stuck, and quantitatively optimizes the design of fracture stage number and spacing under different geological conditions with the goal of fully simulating the horizontal sections. Corresponding design charts are constructed based on the study results to provide references for subsequent design and research. To summarize, this study presents effective strategies for the prevention and control of CT stuck during the CT fracturing in the Junggar Basin.

2. In Situ Stress Field Variation Model During CT Fracturing

During CT fracturing, as hydraulic fractures continue to propagate, the surrounding rock layers, which have not undergone brittle failure, undergo elastic deformation upon receiving pressure from the fluid in the fracture, thereby generating induced stresses. These induced stresses are superimposed onto the original in situ stress field, resulting in a current stress field that varies with the progress of fracturing. Due to the fact that the rocks on both sides of the hydraulic fracture are not damaged and are in an elastic deformation state, based on elasticity theory, this study uses the DDM to calculate the induced stresses

generated by hydraulic fractures, and combines the original in situ stress field to investigate the variation in the reservoir stress field during CT fracturing in the Junggar Basin.

2.1. Displacement Discontinuity Method

The displacement discontinuity method (DDM) was proposed by Crouch [26] and can simulate fractures, cavities, and other units in an infinite elastic medium using discrete elements with discontinuous displacements. Taking a fracture element of length 2*l* within an infinite elastic medium as an example, the schematic diagram of the fracture element, as shown in Figure 1, is established [27]. The displacement on the upper surface of the straight fracture is denoted as $u(x, 0_+)$, and the displacement on the lower surface is denoted as $u(x, 0_-)$. The relationship between the tangential displacement discontinuity D_x, normal displacement discontinuity D_y, and the displacement is given by Equation (1):

$$\begin{cases} D_x = u_x(x, 0_-) - u_x(x, 0_+) \\ D_y = u_y(x, 0_-) - u_y(x, 0_+) \end{cases} \tag{1}$$

where D_x and D_y represent the tangential and normal displacement discontinuities on the fracture element, respectively m; $u_x(x, 0_+)$ and $u_x(x, 0_-)$ are the displacements along the x-axis on the upper and lower surfaces of the fracture, respectively, m; $u_y(x, 0_+)$ and $u_y(x, 0_-)$ are the displacements along the y-axis on the upper and lower surfaces of the fracture, respectively, m.

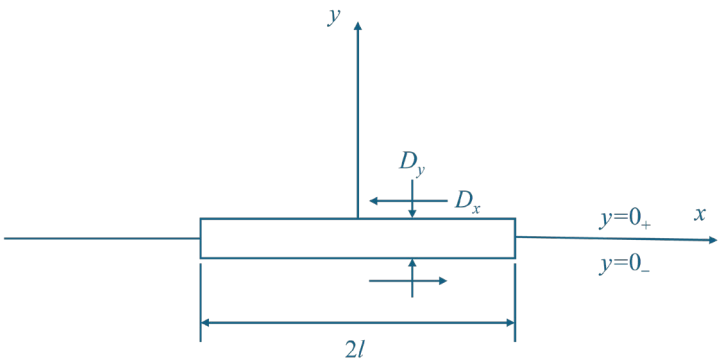


Figure 1. Displacement discontinuity fracture element.

For a homogeneous isotropic linear elastic body, u_x and u_y represent the displacement components in the x and y directions on the fracture surface, respectively [26]:

$$\begin{cases} u_x = D_x\left[2(1-v)f'_y - yf''_{xx}\right] - D_y\left[(1-2v)f'_x + yf''_{xy}\right] \\ u_y = D_x\left[2(1-v)f'_x - yf''_{xy}\right] + D_y\left[(1-2v)f'_x + yf''_{yy}\right] \end{cases} \tag{2}$$

where u_x and u_y represent the horizontal displacement and vertical displacement, m; ν is Poisson's ratio of the reservoir rock, dimensionless.

According to the formulas of elasticity theory, the stress components at any point in the reservoir are shown in Equation (3):

$$\begin{aligned} \sigma_{xx} &= 2GD_x\left(2f''_{xy} + yf'''_{xyy}\right) + 2GD_y\left(2f''_{yy} + yf'''_{xyy}\right) \\ \sigma_{yy} &= 2GD_x\left(-yf'''_{xyy}\right) + 2GD_y\left(f''_{yy} - yf'''_{yyy}\right) \\ \tau_{xy} &= 2GD_x\left(2f''_{yy} + yf'''_{xyy}\right) + 2GD_y\left(-yf'''_{xyy}\right) \end{aligned} \tag{3}$$

where σ_{xx} and σ_{yy} represent the normal stresses in the x and y directions, respectively, MPa; τ_{xy} is the shear stress, MPa; G is the shear modulus, MPa.

The specific expression of the function $f(x, y)$ is shown in Equation (4):

$$\begin{aligned} f(x,y) = -\tfrac{1}{4\pi(1-v)}\Big[y\Big(\arctan\tfrac{y}{x-l} - \arctan\tfrac{y}{x+l}\Big) \\ -(x-l)\ln\sqrt{(x-l)^2+y^2} + (x+l)\ln\sqrt{(x+l)^2+y^2}\Big] \end{aligned} \tag{4}$$

where l represents the half-length of the fracture element, m.

The first, second, and third derivative expressions of the function $f(x, y)$ are as follows:

$$\begin{aligned} f'_x &= \tfrac{1}{4\pi(1-v)}\left\{\ln\left[(x-l)^2+y^2\right]^{1/2} - \ln\left[(x+l)^2+y^2\right]^{1/2}\right\} \\ f'_y &= -\tfrac{1}{4\pi(1-v)}\left[\arctan\tfrac{y}{x-l} - \arctan\tfrac{y}{x+l}\right] \end{aligned} \tag{5}$$

2.2. Induced Stress Calculation Model

Hydraulic fractures can be divided into multiple elements, as shown in Figure 2. The curved boundary is divided into N straight-line elements. For any arbitrary discrete elements i and j, the stress in element i is given by

$$\begin{aligned} \Delta\overset{i}{\sigma}_{xx} &= \sum_{j=1}^{N} \overset{i,j}{I}_{xx}\overset{j}{D}_x + \sum_{j=1}^{N} \overset{i,j}{I}_{xy}\overset{j}{D}_y \\ \Delta\overset{i}{\sigma}_{yy} &= \sum_{j=1}^{N} \overset{i,j}{I}_{yx}\overset{j}{D}_x + \sum_{j=1}^{N} \overset{i,j}{I}_{xy}\overset{j}{D}_y \\ \Delta\overset{i}{\tau}_{xy} &= \sum_{j=1}^{N} \overset{i,j}{I}_{sx}\overset{j}{D}_x + \sum_{j=1}^{N} \overset{i,j}{I}_{sy}\overset{j}{D}_y \end{aligned} \tag{6}$$

where $\Delta\sigma_{xx}$ and $\Delta\sigma_{yy}$ represent the induced stresses in the x and y directions, respectively, MPa; $\Delta\tau_{xy}$ is the tangential induced stress, MPa.

$$\begin{aligned} \overset{i,j}{I}_{xx} &= 2G[2\overset{i,j}{f''_{xy}} + (y_i - y_j)\overset{i,j}{f'''_{xyy}}] \\ \overset{i,j}{I}_{xy} &= 2G[(y_i - y_j)\overset{i,j}{f'''_{yyy}} - \overset{i,j}{f''_{xx}}] \\ \overset{i,j}{I}_{yx} &= 2G[-(y_i - y_j)\overset{i,j}{f'''_{xyy}}] \\ \overset{i,j}{I}_{yy} &= 2G[\overset{i,j}{f''_{yy}} - (y_i - y_j)\overset{i,j}{f'''_{yyy}}] \\ \overset{i,j}{I}_{sx} &= 2G[\overset{i,j}{f''_{yy}} + (y_i - y_j)\overset{i,j}{f'''_{yyy}}] \\ \overset{i,j}{I}_{sy} &= 2G[-(y_i - y_j)\overset{i,j}{f'''_{xyy}}] \end{aligned} \tag{7}$$

where I_{xx}, I_{xy}, I_{yx}, I_{yy}, I_{sx}, and I_{sy} are the stress boundary influence coefficients, with the expressions given as follows:

The displacement of any element i is given by

$$\begin{aligned} \overset{i}{u}_x &= \sum_{j=1}^{N} \overset{i,j}{J}_{xx}\overset{j}{D}_x + \sum_{j=1}^{N} \overset{i,j}{J}_{xy}\overset{j}{D}_y \\ \overset{i}{u}_y &= \sum_{j=1}^{N} \overset{i,j}{J}_{yx}\overset{j}{D}_x + \sum_{j=1}^{N} \overset{i,j}{J}_{yy}\overset{j}{D}_y \end{aligned} \tag{8}$$

where J_{xx}, J_{xy}, J_{yx}, and J_{yy} are the displacement boundary influence coefficients, with the expressions given as

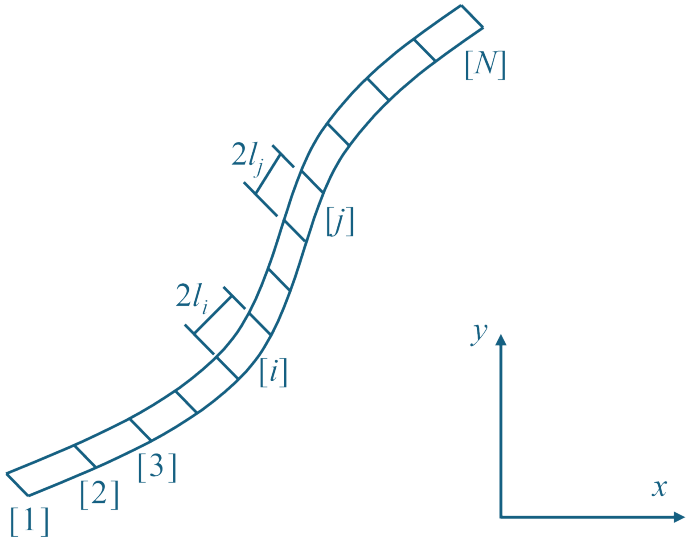


Figure 2. Schematic diagram of hydraulic fracture element division.

$$\begin{aligned} \overset{i,j}{J}_{xx} &= 2(1-\nu)[\overset{i,j}{f'_y} - (y_i - y_j)\overset{i,j}{f''_{xx}}] \\ \overset{i,j}{J}_{xy} &= (1-2\nu)[(y_i - y_j)\overset{i,j}{f''_{xy}} + \overset{i,j}{f'_x}] \\ \overset{i,j}{J}_{yx} &= (1-2\nu)[\overset{i,j}{f'_x} - (y_i - y_j)\overset{i,j}{f''_{xy}}] \\ \overset{i,j}{J}_{yy} &= 2(1-\nu)[\overset{i,j}{f'_y} - (y_i - y_j)\overset{i,j}{f''_{xx}}] \end{aligned} \tag{9}$$

2.3. Current In Situ Stress Field Model

Since both the original in situ stress field and the induced stress field are second-order tensor fields, their components can be linearly superimposed. Therefore, the expression for the current in situ stress field is

$$\begin{bmatrix} \sigma^{c}_{xx} & \tau^{c}_{xy} \\ \tau^{c}_{yx} & \sigma^{c}_{yy} \end{bmatrix} = \begin{bmatrix} \sigma^{p}_{xx} + \Delta\sigma_{xx} & \tau^{p}_{xy} + \Delta\tau_{xy} \\ \tau^{p}_{yx} + \Delta\tau_{yx} & \sigma^{p}_{yy} + \Delta\sigma_{yy} \end{bmatrix} \tag{10}$$

where σ^{c}_{xx}, τ^{c}_{xy}, σ^{c}_{yy}, τ^{c}_{yx} represent the components of the current in situ stress field, MPa; σ^{p}_{xx}, τ^{p}_{xy}, σ^{p}_{yy}, τ^{p}_{yx} represent the components of the original in situ stress field, MPa; $\Delta\sigma_{xx}$, $\Delta\tau_{xy}$, $\Delta\sigma_{yy}$, $\Delta\tau_{yx}$ represent the components of the induced stress field, MPa.

2.4. Numerical Simulation Method

The coupling and assembly of the above models are used to establish the simulation method for the in situ stress field variation during CT fracturing. The specific numerical calculation process is shown in Figure 3.

(1) Parameter input: geological parameters (rock mechanics parameters, in situ stress parameters, etc.), fracturing parameters (fracture length, fracture width, fracture count, etc.);
(2) Induced stress calculation: based on the input rock mechanics parameters and fracturing parameters, calculate the induced stress field generated by the fractures;
(3) Current in situ stress field calculation: the calculated induced stress is superimposed onto the original in situ stress field to calculate the current in situ stress field.

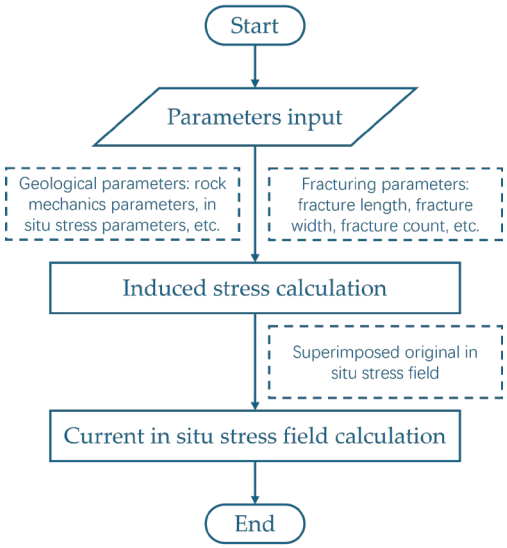


Figure 3. The specific numerical calculation process.

3. Model Application and Analysis

3.1. Model Application

Based on the field construction conditions of CT fracturing in conglomerate and volcanic rock reservoirs in the Junggar Basin, this study applies the CT fracturing in situ stress field variation model established in this research to investigate the in situ stress field changes in the reservoirs of Well H (conglomerate) and Well K (volcanic rock). The goal is to explore the coiled tubing stuck coiled tubing mechanism, with the basic information of wells shown in Table 1.

Table 1. Basic information of Well H and Well K in the Junggar Basin.

Geological and Engineering Parameters	Units	Well H	Well K
Fracturing section length	m	679	797
Young's modulus	GPa	19	31.4
Poisson's ratio		0.26	0.26
Maximum horizontal principal stress	MPa	50	14.5
Minimum horizontal principal stress	MPa	35	9.5
Average perforation spacing	m	33.75	40.3
Stuck stage/Total stages		19/20	15/19

For well H, the induced stress generated during the fracturing process is calculated, and the results are superimposed onto the original in situ stress field to obtain the current stress field near Well H at different fracturing stages (Figure 4). The first stage of fracturing is set at x = 0 m, where the induced stress generated by the hydraulic fracture reduces the horizontal stress difference in the formation along the horizontal well section, but no stress reversal phenomenon is observed (Figure 4a). The stress reversal point is defined as the point where the horizontal stress difference drops to 0 MPa. As shown in Figure 4b–d, after the 2nd to 4th stages of fracturing, the stress reversal points occur at x = 45.23 m, x = 85.43 m, and x = 120.6 m, respectively. The corresponding next-stage fracturing positions are x = 67.5 m, x = 101.3 m, and x = 135.05 m. The distances between the stress reversal points and the next-stage fracturing positions are 20.27 m, 15.87 m, and 14.45 m, respectively. As the number of fracturing stages increases, the distance between the stress reversal points and the next-stage fracturing positions decreases, but the rate of reduction gradually diminishes. Up to the 17th stage of fracturing, the stress reversal point is at x = 573.2 m,

and the 18th stage fracturing position is at x = 573.75 m. It is still outside the stress reversal zone, and no stuck occurs (Figure 4e). After the 18th stage of fracturing, the stress inversion point shifts to x = 608.3 m, while the fracturing point of the next stage (19th stage) is at x = 607.5 m, which falls within the stress inversion zone (Figure 4f). Therefore, CT stuck is highly likely to occur after the 19th stage of fracturing.

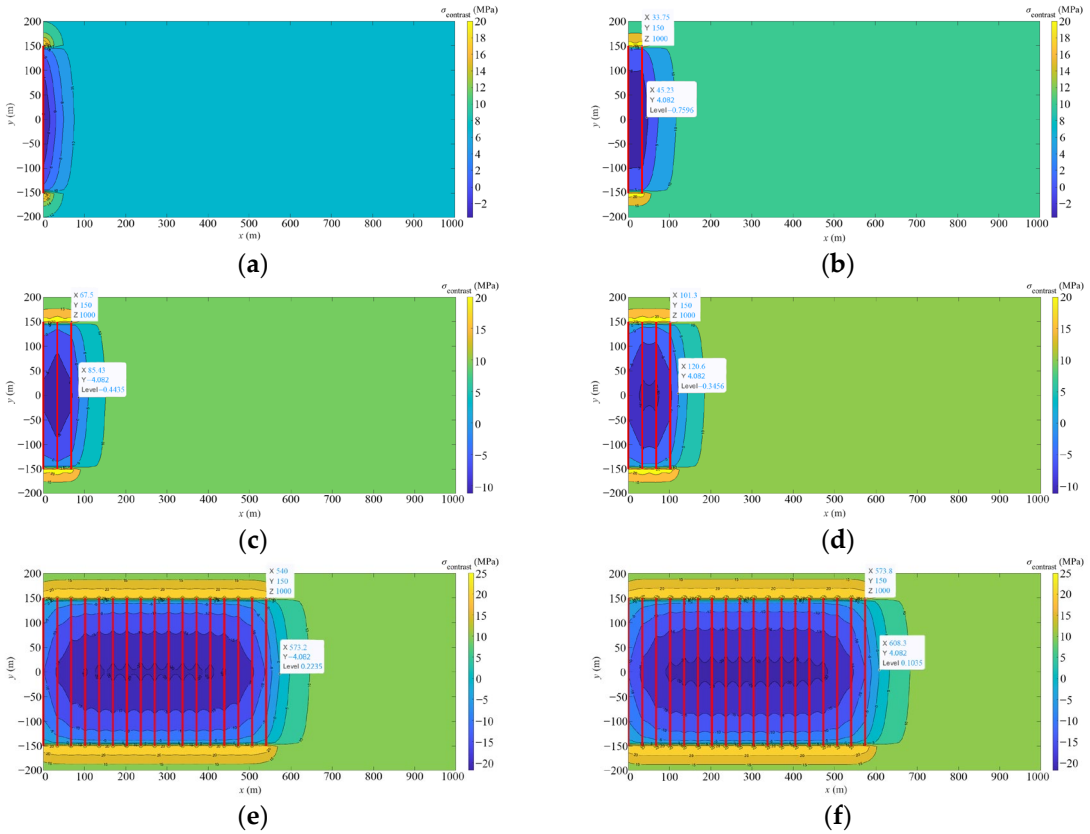


Figure 4. The contour map of the current horizontal stress difference near Well H after fracturing. (**a**) 1st stage; (**b**) 2nd stage; (**c**) 3rd stage; (**d**) 4th stage; (**e**) 17th stage; (**f**) 18th stage.

Based on the calculated results of the current stress field at each fracturing stage for Well H and Well K, the curves showing the variation in horizontal stress difference at the corresponding fracturing positions for each fracturing stage are plotted as shown in Figure 5. The horizontal stress difference at the fracturing positions of the current fracturing stage in the horizontal sections of Well H and Well K shows a rapid change in the early stages of fracturing, followed by a gradual leveling off, exhibiting a nonlinear variation as the fracturing stage increases. Under the influence of induced stress from hydraulic fractures, stress inversion occurs at the 19th fracturing stage position in Well H (Figure 5a), which matches the actual stuck stage. In Well K, stress reversal occurs at the 14th fracturing stage position (Figure 5b), one stage earlier than the actual stuck at the 15th fracturing stage. The stuck positions in both wells are located in the stress inversion zone, demonstrating that the stuck mechanism during CT fracturing is caused by the continuous accumulation of stress induced by hydraulic fractures, leading to stress inversion. It also indicates that the in situ stress field variation model established in this study can be used for conservative prediction of the CT fracturing stuck phenomenon, meeting the on-site demand to avoid stuck during fracturing operations.

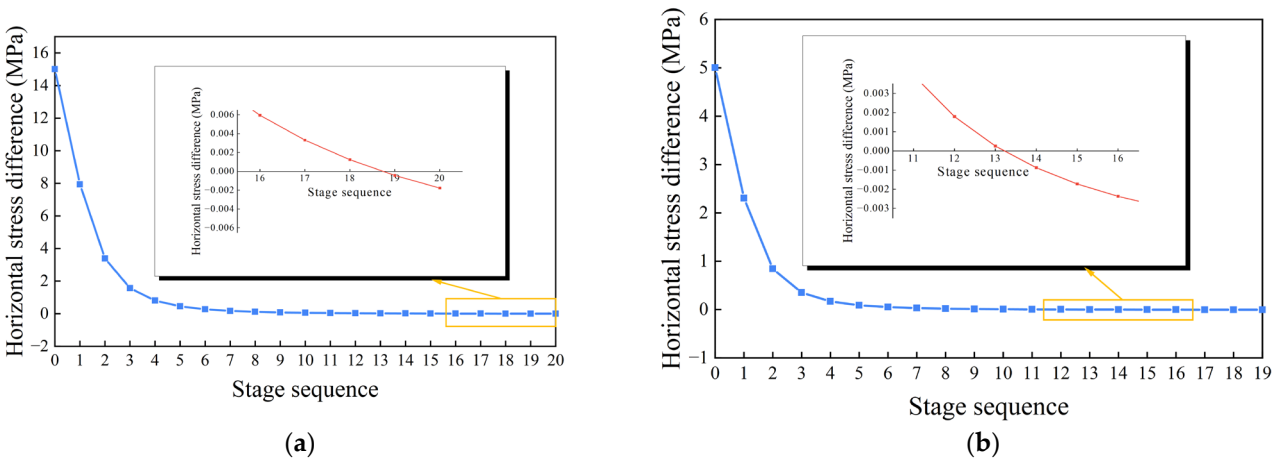


Figure 5. The curve of horizontal stress difference variation at the corresponding fracturing positions for each fracturing stage. (**a**) Well H; (**b**) Well K.

3.2. Sensitivity Analysis

As the number of CT fracturing stages increases, the induced stress field generated by hydraulic fractures continuously accumulates, leading to an expansion of the stress inversion zone. Fracturing within the stress inversion zone significantly increases the risk of stuck coiled tubing. Based on the basic parameters of Well H in Table 1, a study is conducted on the impact of the stage spacing and the original horizontal stress difference on the variation in in situ stress. The fracturing completion index (maximum fracturing stage/design fracturing stage) is established to evaluate whether stuck coiled tubing occurs during the fracturing process. The expression for the fracturing completion index (or fracturing completion ratio) is

$$I_f = \frac{N_m}{N_d} \tag{11}$$

where I_f represents the fracturing completion index, dimensionless; N_m represents the maximum fracturing stage, dimensionless; N_d is the design fracturing stage, dimensionless.

3.2.1. Stage Spacing

Stage spacing refers to the distance between hydraulic fractures, which directly affects the intensity and range of induced stress accumulation. Stress inversion caused by the induced stress will lead to CT stuck during the fracturing process. The variations in the in situ stress field in the horizontal section of the well were simulated for stage spacings of 25 m, 28 m, 33.75 m, 50 m, and 100 m, as the number of stages in the CT fracturing increased. The curves of the fracturing completion index and fracturing section length with varying stage spacing are shown in Figure 6. The fracturing completion index increases with the stage spacing until it reaches 100%. The fracturing section length initially increases and then decreases as the stage spacing increases. This is because, with a fixed horizontal well length, when the stage spacing is too large, the number of fracturing stages decreases, and the longer portion of the horizontal section near the end is difficult to fracture, leading to a reduction in the fracturing section length.

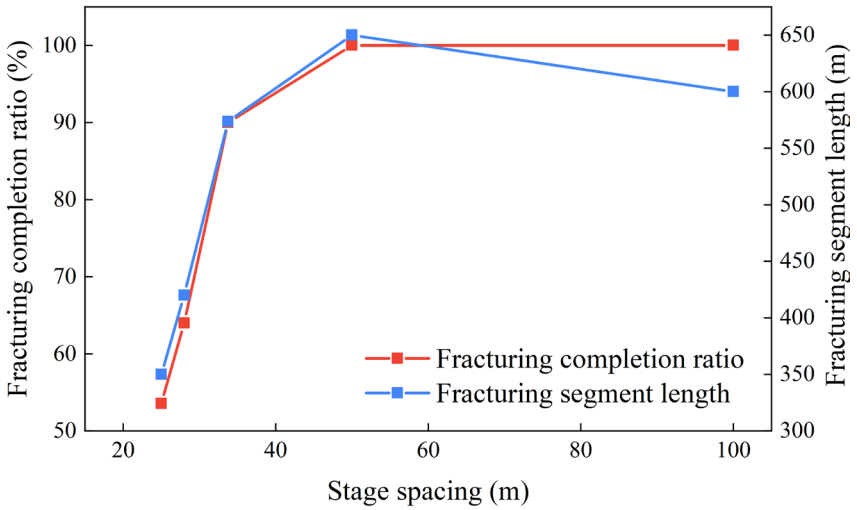


Figure 6. The curve of fracturing completion ratio and fracturing section length with varying stage spacing.

3.2.2. Original Horizontal Stress Difference

The original horizontal stress difference reflects the ability of the in situ stress field to resist the influence of induced stresses from hydraulic fractures. If the original horizontal stress difference is insufficient to resist the impact of induced stresses, stress inversion is more likely to occur, leading to CT stuck during the fracturing process. The variations in the stress field of the horizontal wellbore section with the increase in the number of CT fracturing stages are simulated for original horizontal stress differences of 10 MPa, 15 MPa, and 20 MPa, respectively. The curves of the fracturing completion index and fracturing segment length with varying original horizontal stress difference are shown in Figure 7. The fracturing completion index and fracturing section length both increase with the increase in original horizontal stress difference. This is because, with a fixed horizontal well length and stage spacing, the more stages completed, the higher the fracturing completion index and the longer the fracturing section length.

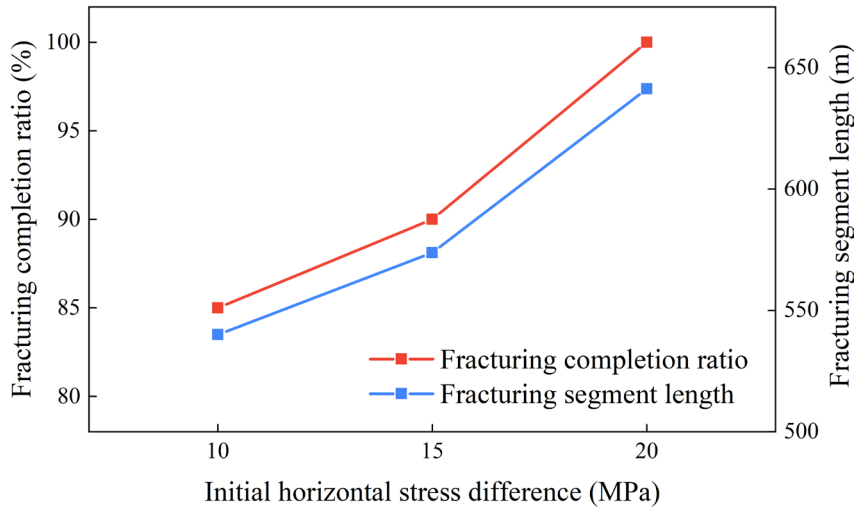


Figure 7. The curve of fracturing completion ratio and fracturing section length with varying original horizontal stress difference.

3.3. Fracturing Parameter Design Diagram

Through the analysis of the variation law of the in situ stress field, it is found that stage spacing and original horizontal stress difference have a significant impact on the location of pipe stuck during CT fracturing. Combining the geological and engineering characteristics of CT fracturing in the Junggar Basin, the in situ stress field variation model established in this paper is used to simulate the variations in the in situ stress field during CT fracturing operations.

Based on whether the in situ stress reverses, the CT fracturing design for sandstone and volcanic reservoirs is quantitatively optimized for stage spacing and number of stages under varying horizontal section lengths and original horizontal stress differences. The stage spacing and number of stages design charts (Figures 8 and 9) provide effective strategies for the prevention and control of the stuck coiled tubing phenomenon during fracturing operations.

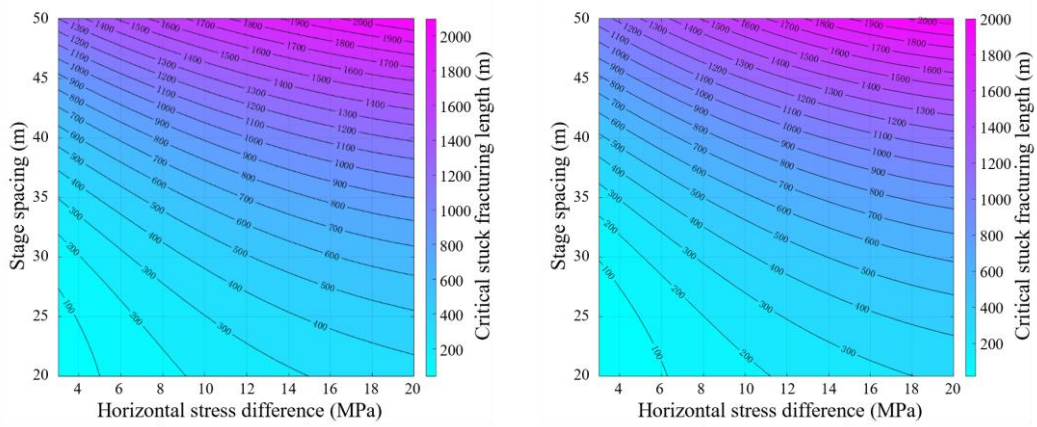


Figure 8. Stage spacing design chart. (**a**) Conglomerate reservoir; (**b**) Volcanic rock reservoir.

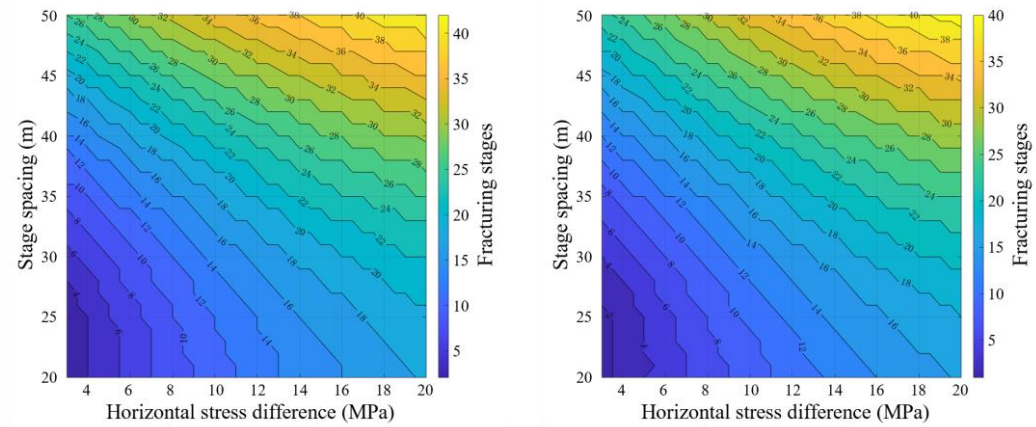


Figure 9. Number of stages design chart. (**a**) Conglomerate reservoir; (**b**) Volcanic rock reservoir.

4. Conclusions

This study is based on elastic mechanics and utilizes the DDM to establish an in situ stress field variation model for CT fracturing. By simulating the in situ stress field variations during the CT fracturing process in the Junggar Basin, this study investigated the mechanisms of stuck coiled tubing and the variation laws of in situ stress reversal. With

the goal of fully simulating the horizontal sections, this study quantitatively optimized the design of fracturing stage spacing and stage numbers under different geological conditions, and then proposed corresponding design parameter charts. The main conclusions are as follows:

(1) During the CT fracturing process in the Junggar Basin, the induced stress generated by hydraulic fractures reduces the horizontal stress difference in the formation. As the number of fracturing stages increases, the impact of induced stress on the in situ stress field becomes more significant, even leading to stress reversal phenomena.
(2) Stuck coiled tubing is mainly caused by stress reversal induced by hydraulic fractures. The in situ stress field variation model established in this study can be used to predict stuck coiled tubing incidents during the CT fracturing.
(3) The fracturing completion index increases with the increase in stage spacing and original horizontal stress difference. The fracturing section length increases with stage spacing up to a point, then decreases, while it increases with the original horizontal stress difference.
(4) The parameter design charts developed in this study can reasonably design the fracturing stage spacing and number of stages, providing effective countermeasures to prevent stuck during the fracturing process.

Author Contributions: Methodology, R.L.; Resources, H.Y., C.G. and X.C.; Writing—original draft, Q.R.; Writing—review & editing, L.R. and Q.D. All authors have read and agreed to the published version of the manuscript.

Funding: This research received no external funding.

Data Availability Statement: The original contributions presented in this study are included in the article. Further inquiries can be directed to the corresponding author.

Conflicts of Interest: Authors Hongcheng Yin, Changyong Guo and Xianjiang Chen were employed by the Development Company, Xinjiang Oilfield Company, Author Qinyue Deng was employed by the Southwest Oil & Gas field Company. The remaining authors declare that the research was conducted in the absence of any commercial or financial relationships that could be construed as a potential conflict of interest.

References

1. Taner, I.; Kamen-Kaye, M.; Meyerhoff, A.A. Petroleum in the Junggar Basin, Northwestern China. *J. Southeast Asian Earth Sci.* **1988**, *2*, 163–174. [CrossRef]
2. Hu, S.; Wang, X.; Cao, Z.; Li, J.; Gong, D.; Xu, Y. Formation Conditions and Exploration Direction of Large and Medium Gas Reservoirs in the Junggar Basin, Nw China. *Petrol. Explor. Dev.* **2020**, *47*, 266–279. [CrossRef]
3. Yang, H.; Ni, H.; Wu, T. Research and Application of Fracturing Process for Low Permeability Reservoir of Triassic in Junggar Basin. In Proceedings of the International Conference on Environmental Prevention and Pollution Control Technologies, Sanya, China, 10–12 January 2020.
4. Yu, Z.; Wang, Z.; Jiang, Q.; Wang, J.; Feng, Y.; Zheng, J.; Baffour, B.A. Evaluation of low Permeability Conglomerate Reservoirs Based on Petrophysical Facies: A Case Study from the Triassic Baikouquan Formation, Northern Mahu Sag, Junggar Basin, China. *J. Petrol Sci. Eng.* **2022**, *219*, 111082. [CrossRef]
5. Xiao, M.; Wu, S.; Yuan, X.; Cao, Z.; Xie, Z. Diagenesis Effects on the Conglomerate Reservoir Quality of the Baikouquan Formation, Junggar Basin, China. *J. Petrol Sci. Eng.* **2020**, *195*, 107599. [CrossRef]
6. Wu, X.; Guo, Q.; Zhang, W.; He, D.; Qi, X.; Li, D. Characteristics of Volcanic Reservoirs and Hydrocarbon Accumulation of Carboniferous System in Junggar Basin, China. *J. Earth Sci.* **2021**, *32*, 972–985. [CrossRef]
7. Yang, G.; Zhang, S.; Wang, J.; Li, N.; Ma, X.; Zou, Y. Effect of Multiple Flow Pulses on Hydraulic Fracture Network Propagation in Naturally Fractured Volcanic Rock. *Energies* **2020**, *13*, 633. [CrossRef]
8. Shi, S.; Zhuo, R.; Cheng, L.; Xiang, Y.; Ma, X.; Wang, T. Fracture Characteristics and Distribution in Slant Core from Conglomerate Hydraulic Fracturing Test Site (Chfts) in Junggar Basin, Northwest China. *Processes* **2022**, *10*, 1646. [CrossRef]

9. Liu, Q. Exploration and Practice of New Technology for Development of Carboniferous Large-Span Block Reservoir in Well Dzungar Basin 403. In Proceedings of the International Field Exploration and Development Conference, Xi'an, China, 16–18 November 2022.
10. Shah, S.; Zhou, Y.; Bailey, M.; Hernandez, J. Correlations to Predict Frictional Pressure Loss of Hydraulic-Fracturing Slurry in Coiled Tubing. *SPE Prod. Oper.* **2009**, *24*, 381–395. [CrossRef]
11. Algadi, O.; Filyukov, R.; Luna, D. Multistage Hydraulic Fracturing Using Coiled Tubing-Activated Frac Sleeves: Case Study from the Permian Basin. In Proceedings of the SPE Annual Technical Conference and Exhibition, Amsterdam, The Netherlands, 27–29 October 2014.
12. Shi, H.; Ji, Z.; Zhao, H.; Song, H.; Chen, Z. Investigations into the coiled tubing partial underbalanced drilling (CT-PUBD) technique for drilling hard formations. *Petrol Sci.* **2018**, *15*, 830–840. [CrossRef]
13. Gulrajani, S.; Olmstead, C.C. Coiled Tubing Conveyed Fracture Treatments: Evolution, Methodology and Field Application. In Proceedings of the SPE Eastern Regional Meeting, Charleston, WV, USA, 21–22 October 1999.
14. Gavin, W. Fracturing through Coiled Tubing-Recent Developments and Case Histories. In Proceedings of the SPE/ICoTA Coiled Tubing Roundtable, Houston, TX, USA, 5–6 April 2000.
15. Mcdaniel, B.; Willett, R.; East, L.; Rosato, J.; Surjaatmadja, J. Coiled-Tubing Deployment of Hydrajet-Fracturing Technique Enhances Safety and Flexibility, Reduces Job Time. In Proceedings of the SPE Annual Technical Conference and Exhibition, Houston, TX, USA, 26–29 September 2004.
16. Shah, S.N.; Jain, S. Coiled Tubing Erosion During Hydraulic Fracturing Slurry Flow. *Wear* **2008**, *264*, 279–290. [CrossRef]
17. Huang, Z.; Li, G.; Tian, S.; Song, X.; Sheng, M.; Shah, S. *Abrasive Water Jet Perforation and Multi-Stage Fracturing*, 1st ed.; Gulf Professional Publishing: Houston, TX, USA, 2017; pp. 153–190.
18. Sun, S.; Liu, J.; Sang, R.; Zhao, K. Experimental Study of Flow Friction Behavior in Coiled Tubing. *Energy Rep.* **2022**, *8*, 187–196. [CrossRef]
19. Xu, A.; Dou, Y.; Feng, C.; Zheng, J.; Cui, X. Coiled Tubing Erosion Prediction and Fracturing Fluid Parameters Optimization During Hydraulic Jet Fracturing. *J. Fail Anal. Prev.* **2022**, *22*, 1276–1292. [CrossRef]
20. Kazakov, S.; Rispler, K. Optimizing and Managing Coiled Tubing Frac Strings. In Proceedings of the SPE/ICoTA Coiled Tubing Roundtable, Houston, TX, USA, 5–6 April 2000.
21. Wang, W.; Long, S.; Su, M.; Ma, Y.; Huang, W. Design and Test of Hydraulic Bottom Seal Fracturing Tool for Coiled Tubing. In Proceedings of the International Petroleum and Petrochemical Technology Conference, Beijing, China, 25–27 March 2024.
22. Liu, S.; Zhou, H.; Xiao, H.; Gan, Q. A New Theoretical Model of Low Cycle Fatigue Life for Coiled Tubing Under Coupling Load. *Eng. Fail Anal.* **2021**, *124*, 105365.
23. Zhang, J.; Yin, G.; Fan, Y.; Zhang, H.; Tian, L.; Qin, S.; Zhu, D. The Helical Buckling and Extended Reach Limit of Coiled Tubing with Initial Bending Curvature in Horizontal Wellbores. *J. Petrol Sci. Eng.* **2021**, *200*, 108398. [CrossRef]
24. Vechietti, M.; Di, B.B.; Krasuk, R.M.; Mirande, J.M.; Franco, D.E.; Trujillo, S.; Palombizio, G.; Jahn, F.; Carreno, N. The Challenges to Retrieve a Stuck Coiled-Tubing Pipe Without Downhole Check Valves in a High-Pressure Well: A Case Study from Argentina. In Proceedings of the SPE/ICoTA Well Intervention Conference and Exhibition, The Woodlands, TX, USA, 22–23 March 2022.
25. Khan, J.A.; Irfan, M.; Irawan, S.; Yao, F.K.; Abdul Rahaman, M.S.; Shahari, A.R.; Glowacz, A.; Zeb, N. Comparison of Machine Learning Classifiers for Accurate Prediction of Real-Time Stuck Pipe Incidents. *Energies* **2020**, *13*, 3683. [CrossRef]
26. Crouch, S. Solution of Plane Elasticity Problems by the Displacement Discontinuity Method. I. Infinite Body Solution. *Int. J. Numer. Meth. Eng.* **1976**, *10*, 301–343. [CrossRef]
27. Morris, J.P.; Blair, S.C. An Efficient Displacement Discontinuity Method Using Fast Multipole Techniques. In Proceedings of the 4th North American Rock Mechanics Symposium, Seattle, WA, USA, 31 July–3 August 2000.

Disclaimer/Publisher's Note: The statements, opinions and data contained in all publications are solely those of the individual author(s) and contributor(s) and not of MDPI and/or the editor(s). MDPI and/or the editor(s) disclaim responsibility for any injury to people or property resulting from any ideas, methods, instructions or products referred to in the content.